Effect of Wafer Bow and Etch Patterns in Direct Wafer Bonding

K.T. Turner and S.M. Spearing
Massachusetts Institute of Technology
Cambridge, MA 02139 USA

Abstract— **Direct wafer bonding has been identified as an enabling technology for microelectromechanical systems (MEMS). As the complexity of devices increase and the bonding of multiple patterned wafers is required, there is a need to understand the factors that lead to bonding failure. Bonding relies on short-ranged surface forces, thus flatness deviations of the wafers may prevent bonding. Bonding success is determined by whether or not the surface forces are sufficient to overcome the flatness deviations and deform the wafers to a common shape. A general bonding criterion based on this fact is developed by comparing the strain energy required to deform the wafers to the surface energy that is dissipated as the bond is formed. The bonding criterion is used to examine the case of bonding bowed wafers with etch patterns on the bonding surface. An analytical expression for the bonding criterion is developed using plate theory for the case of bowed wafers. Then, the criterion is implemented using finite element analysis, to demonstrate its use and to validate the analytical model. The results indicate that wafer thickness and curvature are important in determining bonding success and that the bonding criterion is independent of wafer diameter. Results also demonstrate that shallow etched patterns can make bonding more difficult while deep features, which penetrate through an appreciable thickness of the wafer, may facilitate bonding. Design implications of the model results are discussed in detail. Preliminary results from experiments designed to validate the model, agree with the trends seen in the model, but further work is required to achieve quantitative correlation.**

Index Terms— **direct bonding, MEMS, etch pattern, wafer bonding, wafer bow**

I. Introduction

WAFER bonding has emerged as an important technology for the manufacture of microelectromechanical systems (MEMS). It greatly enhances design flexibility and permits the construction of three-dimensional mechanical structures through the lamination of multiple etched wafers. Direct wafer bonding, which is a process in which clean highly polished wafers can be bonded with no intermediate layer, has proven particularly attractive because it allows bonds with high temperature stability and strengths that approach that of the wafers being bonded to be fabricated. Commercial products based on wafer bonding are currently produced, [1], and numerous devices that are still being developed rely on the technology as well. Figure 1(a), which shows a miniature silicon gas turbine engine, is an example of a MEMS device that relies on direct wafer bonding. The device is fabricated by patterning and etching six silicon wafers, which are subsequently bonded. The successful fabrication of the device requires five wafer bonds with high yield in each step. Figure 1(b) is an illustration of a poor wafer bond and demonstrates that failure during the bonding process can render the devices unusable. Bonding difficulties, such as those illustrated in Fig. 1(b), are becoming increasingly more common as designers move to processes with more complicated etch patterns and multiple wafer bonds. The current work seeks to understand the factors that lead to bonding failure and to develop modeling techniques that permit the intelligent design of device geometry, pattern layouts, and process flows for wafer bonded devices. The focus of the work reported herein is on the effect of wafer-bow and etch patterns on the bonding process.

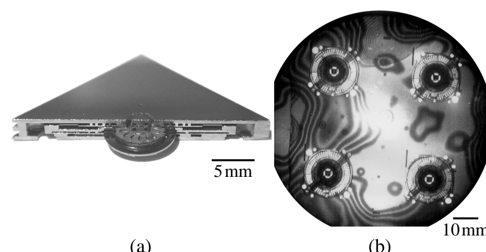

Fig. 1. A six-wafer miniature silicon gas turbine engine. (a) A device that has been cross-sectioned to illustrate the multi-wafer architecture [2]. (b) An infrared transmission image of a wafer bonded stack (four devices) showing bonding failure [3]. The fringes and dark regions indicate un-bonded regions.

Direct wafer bonding is not a new process. It was first reported as a means to bond silicon wafers in 1985 by Lasky et al., [4]. The process was developed over the next decade as a means to fabricate silicon-on-insulator (SOI) substrates for microelectronics and remains one of the dominant techniques used in the industry today. As part of this technology development, numerous researchers have investigated the factors that lead to bonding failure, the majority of this work is documented in a book on semiconductor wafer bonding [5], and several review articles [6], [7]. Much of the work has focused on surface chemistry and limited attention has been focused on the effect of flatness deviations and etch patterns. Stengl et al. [8] and Tong et al. [9] examined the effect of long wavelength surface waviness on bonding through simple mechanics considerations. More recently Yu and Suo [10] performed a detailed analysis of the problem of the contacting

Manuscript received November 8, 2002. This work was supported in part by the Singapore MIT Alliance (SMA MOU 11/6/98) and Cambridge MIT institute (CMI–059/P-IR(FT)MEMS).
e-mail: kturner@mit.edu, spearing@mit.edu

of two wafers with wavy surfaces and Gui et al. [11] looked at the role that surface roughness plays. While these analysis have provided valuable insight into the factors that may prevent bonding, they have only addressed limited cases of flatness deviations. A general criterion for bonding has not been established and the role of etch patterns in direct bonding has been neglected. The primary reason for this, is that the motivation behind the previous work was bonding for SOI, in which the bonding processes are much simpler - in that the wafers are un-patterned and multiple wafer bonds are rarely required. The unique requirements of the wafer bonding processes employed in MEMS device fabrication requires a better understanding of the bonding process.

In the present work, a general bonding criterion is first developed. This criterion is then employed to examine the effect of wafer bow on bonding. The case of bonding blank wafers is initially examined and then the model is extended to account for pattern effects. The model is developed using linear plate theory and is also evaluated using finite element analysis. Results for bonding blank wafers and patterned wafers are discussed in detail. Implications for device and process design are highlighted. Finally, validation experiments are described and preliminary experimental results discussed.

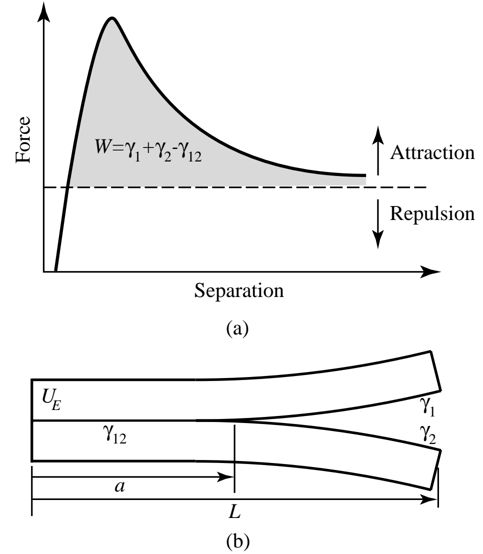

Fig. 2. (a) The force separation curve for two surfaces. The area under the curve represents the work of adhesion. (b) The change in system energy as two surfaces are bonded. Surface energy (γ_1, γ_2) is lost, interface energy (γ_{12}), and strain energy (U_E) are gained as a increases.

II. BONDING CRITERION

It is well established that the key mechanism in the room temperature contacting step of direct bonding is the formation of weak interatomic bonds, such as van der Waals and hydrogen bonds [5]. These forces are short range and as such wafer bonding is typically accomplished by pressing the wafers into contact at one point, from which the bond front advances and 'zips' up the interface. For analysis, it is useful to represent these forces in terms of surface energies as shown in Fig. 2(a). As is illustrated in Fig. 2(b), as the interface advances, surface energy is lost and interface energy is gained. The net change in energy due to the formation of the bonded interface, which known as the Dupré work of adhesion, W, can be expressed in terms of the surface energies of the two solids, γ_1 and γ_2, and the interface energy, γ_{12},

$$W = \gamma_1 + \gamma_2 - \gamma_{12}. \tag{1}$$

When bonding two solids of the same material, $\gamma_{12} = 0$, $\gamma_1 = \gamma_2$, and the work of adhesion reduces to $W = 2\gamma_1$. The work of adhesion represents the energy available per unit area to bond two surfaces. If the geometry of the wafer surfaces perfectly match one another, then bonding will occur given that the work of adhesion is positive. However, wafer surfaces rarely match perfectly due to flatness deviations and the requirement for bonding is that the work of adhesion must be sufficient to cause the wafers to deform elastically to a common shape. If we take the structure shown in Fig. 2(b) to have a constant width, B, the total energy in the system, U_T, as a function of bond front position, a, is given as

$$U_T = U_E + aB\gamma_{12} + (L - a)B(\gamma_1 + \gamma_2). \tag{2}$$

The elastic strain energy, U_E, is accumulated in the wafers as they conform to one another and is in general a function of the bond front position. The bond front will propagate until the system is in equilibrium, this occurs when the total system energy is minimized, $dU_T/da = 0$. Evaluating this condition using Eq. (2) and writing in terms of the work of adhesion, the equilibrium condition is expressed as

$$\frac{1}{B}\frac{dU_E}{da} = W. \tag{3}$$

This can be generalized to three dimensional situations where the width is not uniform by taking the derivative of the strain energy with respect to the area of the interface, A. Noting that the bond will propagate to the equilibrium position, the bonding criterion can be written as

$$\frac{dU_E}{dA} \leq W. \tag{4}$$

The term dU_E/dA is a function of the wafer geometry and material properties and will be referred to as the strain energy accumulation rate. Equation (4) is the basic criterion for bonding and determines whether or not the bond front will advance. It is important to recognize that this is a criterion for bond front advance, thus the surfaces must be in contact at a point from which the bond front can grow for this criterion to apply. The criterion is equivalent to the familiar Griffith criterion for fracture, but rather than looking at a crack propagating, the current problem is concerned with a crack closing. The requirement that the wafers be in contact at a point is directly analogous to the requirement that a sharp crack be present when using the Griffith criterion.

This criterion is general and can be employed to evaluate the effect of a range of flatness deviations on bonding success. The key to using the criterion is to develop an expression for the strain energy as a function of bond front advance. Depending on the nature of the flatness deviation, this may be developed analytically or determined numerically. In the following sections, the criterion is evaluated for the case of

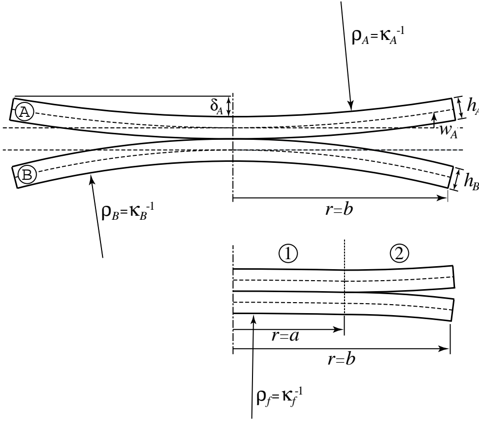

Fig. 3. Schematic of bonding two bowed wafers showing assumed geometry and notation used. As shown, κ_A is a positive curvature and κ_B is a negative curvature.

bowed wafers using an analytical model based on plate theory and numerically using finite element analysis.

III. Wafer Bow

Semiconductor wafers are typically highly polished with very smooth surfaces (r.m.s. roughness less than 1 nm), but are not necessarily flat across the wafer. The presence of height variations of tens of nanometers across millimeter scale wavelengths and flatness variations of microns across the wafer are well documented. One such type of flatness deviation, that may be a result of the wafer manufacturing process or the presence of a residually stressed film, is wafer bow. Wafer bow, which is illustrated schematically in Fig. 3, generally refers to wafers in the shape of a spherical shallow cap. Wafer bow is typically characterized in terms of the curvature of the wafer, κ, or the "bow," δ.

A. Analytical formulation

Figure 3 schematically illustrates the process of bonding two bowed wafers. The geometry of the wafers, denoted A and B, is defined in terms of their curvatures, κ_A and κ_B, their thicknesses, h_A and h_B, and their outer diameter, b (it is assumed they both have the same outer diameter). The curvature of either wafer can be negative or positive. As drawn in Fig. 3, κ_A is a positive curvature and κ_B is negative. The wafers are assumed to be isotropic and their elastic behavior is defined in terms of Young's modulus, E_A and E_B, and Poisson's ratio, ν_A and ν_B. Contact between the wafers is initially made at the center and it is assumed that the bond front propagates axisymmetrically outward. The bond front position is denoted as a. As the bond front advances, the wafers deform to a common curvature, κ_f. It should be noted that due to the requirement that contact is initially made at the center, the current analysis is limited to cases where $\kappa_B < \kappa_A$.

In order to derive the bonding criterion, an expression for the strain energy in the wafers as a function of bond front position must be developed. This is done here by first solving for the deflections of the wafers as the bond front advances and then using these deflections to directly compute the strain energy. To solve the problem, the plate is divided into two sections, 1 and 2, as shown in Fig. 3. The radius of curvature of the wafers is large, thus the shape of the wafers can be approximated as a parabola. The initial shapes, w_{oi}, of the wafers are given as

$$w_{oi} = \left(\frac{1}{2\rho_i}\right) r^2 = \frac{1}{2}\kappa_i r^2, \tag{5}$$

where the subscript i is used to denote the wafer, either A or B. The shape of the wafers after bonding can be expressed in terms of the final curvature or in terms of the initial shape and the deflection, $\bar{w}_i$, of the wafer during the bonding process,

$$w_f = \frac{1}{2}\kappa_f r^2 = w_{oi} + \bar{w}_i. \tag{6}$$

In section 1 of the wafer, the bonded section, $(0 \le r \le a)$, the deflection can be solved for directly from Eqs. (5) and (6),

$$\bar{w}_{1i} = \frac{1}{2}(\kappa_f - \kappa_i)r^2. \tag{7}$$

The deformation in section 1 leads to stresses in section 2. Using the governing equation for the plate and the appropriate boundary conditions, the deflection in section 2 as a function of bond front position is determined,

$$\bar{w}_{2i} = \frac{1}{2}\frac{a^2(\kappa_f - \kappa_i)}{b^2(1+\nu_i) + a^2(1-\nu_i)} \cdot \left\{(1-\nu_i)r^2 + 2(1+\nu_i)b^2\left[ln\left(\frac{r}{a}\right) + \frac{1}{2}\right]\right\}. \tag{8}$$

Details of the derivation of Eq. (8) are provided in ref [12]. The deflection of the wafers as a function of bond front position is fully described by Eqs. (7) and (8). Using these, the strain energy in each wafer can be calculated directly using, [13]:

$$U_i = \pi D_i \int_0^b \left[\left(\bar{w}_i'' + \frac{1}{r}\bar{w}_i'\right)^2 - \frac{2(1-\nu)\bar{w}_i''\bar{w}_i'}{r}\right] r dr. \tag{9}$$

Where the $'$ denotes d/dr and D_i is the plate rigidity:

$$D_i = \frac{E_i h_i^3}{12(1-\nu_i^2)}. \tag{10}$$

Using Eq. (9) to calculate the strain energy in each section and summing, the total strain energy in each wafer, U_{Ei}, is:

$$U_{Ei} = \frac{\pi}{6}E_i h_i^3(\kappa_f - \kappa_i)^2 \cdot \frac{a^2 b^2}{(1-\nu_i)[b^2(1+\nu_i) + a^2(1-\nu_i)]}. \tag{11}$$

When the bond front propagates axisymmetrically, the bonding criterion is calculated as

$$\frac{dU_{Ei}}{dA} = \frac{dU_{Ei}}{da}\frac{da}{dA}. \tag{12}$$

For the case of blank wafers,

$$A = \pi a^2, \tag{13}$$

$$\frac{da}{dA} = \frac{1}{2\pi a}. \tag{14}$$

Using Eqs. (11), (12), and (14) and defining a non-dimensional parameter, $R = a/b$, that indicates the relative bond front

advance, the expression for the strain energy accumulation rate in each wafer is written as,

$$\frac{dU_{Ei}}{dA} = \frac{1}{6}E_i h_i^3(\kappa_f - \kappa_i)^2 \cdot \frac{(1+\nu_i)}{(1-\nu_i)}\frac{1}{\left[(1+\nu_i)+R^2(1-\nu_i)\right]^2}. \quad (15)$$

While this expression is for the strain energy accumulation rate, it is difficult to use because in general the final curvature, κ_f, is not known. The final curvature of the bonded pair is a function of the curvatures, elastic properties, and thicknesses of both wafers. The final curvature of the bonded pair is determined by equilibrium and can be determined by looking at the curvature that yields the minimum strain energy. The strain energy of the system, U_E, is the sum of the strain energy in each wafer,

$$U_E(\kappa_f, a) = U_{EA} + U_{EB}. \quad (16)$$

For a given bond front position, a, the curvature that yields the minimum stain energy is determined by

$$\frac{dU_E}{d\kappa_f} = 0. \quad (17)$$

Using Eqs. (11) and (16), the equilibrium curvature can be determined by solving Eq. (17) for κ_f. When $\nu_A = \nu_B$, which is common in many scenarios, the final curvature is independent of Poisson's ratio and R,

$$\kappa_f|_{\nu_A=\nu_B} = \frac{E_A h_A^3\kappa_A + E_B h_B^3\kappa_B}{E_A h_A^3 + E_B h_B^3}. \quad (18)$$

When $\nu_A \neq \nu_B$, the curvature is not uniform across the wafer, details regarding this case are included in Ref. [12].

Using Eqs. (15) and (18), the strain energy accumulation rate for bonding two bowed wafers can be written as:

$$\frac{dU_E}{dA} = \frac{1}{6}\frac{E_A E_B h_A^3 h_B^3}{E_A h_A^3 + E_B h_b^3}(\kappa_A - \kappa_B)^2 \cdot \frac{(1+\nu)}{(1-\nu)}\frac{1}{\left[(1+\nu)+R^2(1-\nu)\right]^2}. \quad (19)$$

This expression gives the strain energy accumulation rate in terms of the geometry and material properties of the two wafers being bonded.

B. *Finite element formulation*

While the bonding criterion may be derived using simple plate theory for the case of bowed wafers, many geometries are not amenable to an analytical formulation. For this reason, it is desirable to have a method that permits the evaluation of the bonding criterion for a range of geometries. Finite element analysis permits this and in order to demonstrate its use in the this context, the bonding criterion for bowed wafers has been evaluated. A finite element model using the commercial package ABAQUS [14] was constructed of the problem presented in Fig. 3. Each wafer was meshed with 800 8-node axisymmetric continuum elements arranged in a rectangular grid with 4 nodes through the thickness of the wafer. Displacements were applied at the nodes at the interface to bring the surfaces of two wafers together. To evaluate the strain energy as a function of interface position, the model was solved multiple times with an increasing number of nodes at the interface being 'bonded' (displaced) in each model run. Strain energy values for each case were recorded and strain energy as a function of bond front position was obtained. The bonding criterion was evaluated using numerical differentiation to approximate the derivative,

$$\frac{dU_E}{dA} = \frac{U_{j+1} - U_j}{\pi(a_{j+1}^2 - a_j^2)}, \quad (20)$$

where the subscript, j, denotes solutions with different numbers of nodes at the interface being displaced. This permits the strain energy accumulation rate as a function of bond front position to be evaluated.

IV. Etch Pattern

In MEMS applications, wafers are typically etched prior to bonding. Etching prior to bonding, while adding design flexibility, may also make bonding more difficult. The effect of some basic etch patterns are considered here to examine the relative impact of etched features on the bonding surface. The basic patterns considered here are illustrated in Fig. 4. In addition to the different patterns, there are two general types of etch features that are considered as bounding cases: shallow and deep. Shallow features refer to etches that are a few microns deep in a substrate hundreds of microns thick, while deep features refer to etches that penetrate through an appreciable thickness of the wafer.

The primary effect of shallow features is to reduce the bonding area and hence the energy available to deform the wafers. The fact that they are shallow means that while the bonding area is reduced, the stiffness of the wafer, and thus the strain energy required to deform the wafers, is not affected significantly by the presence of the features. This effect is incorporated into the current analysis when calculating the strain energy accumulation rate. In the case of axisymmetric bond front propagation, the bonding criterion is evaluated using Eq. (12), where the term da/dA accounts for how the bond area changes as a function of bond front position.

The case presented earlier was for blank wafers, where the bonded area is described by $A = \pi a^2$. The first pattern considered here, shown in Fig. 4(a), is a randomly distributed arrangement of circular holes. The features are assumed to be sufficiently small and distributed such the bonded area is described by

$$A = p_a \pi a^2, \quad (21)$$

where p_a is the fraction of bonding area remaining, and may be expressed in terms of the etch area fraction, c_a, as $p_a = 1 - c_a$. The strain energy accumulation rate is calculated by evaluating the term da/dA and using Eq. (12) to evaluate the strain energy release rate. The adjusted strain energy accumulation rate can be written in terms of the strain energy accumulation rate of un-patterned wafers, $(dU/dA)_{blank}$.

$$\left(\frac{dU_E}{dA}\right)_{distributed} = \frac{1}{p_a}\left(\frac{dU_E}{dA}\right)_{blank}. \quad (22)$$

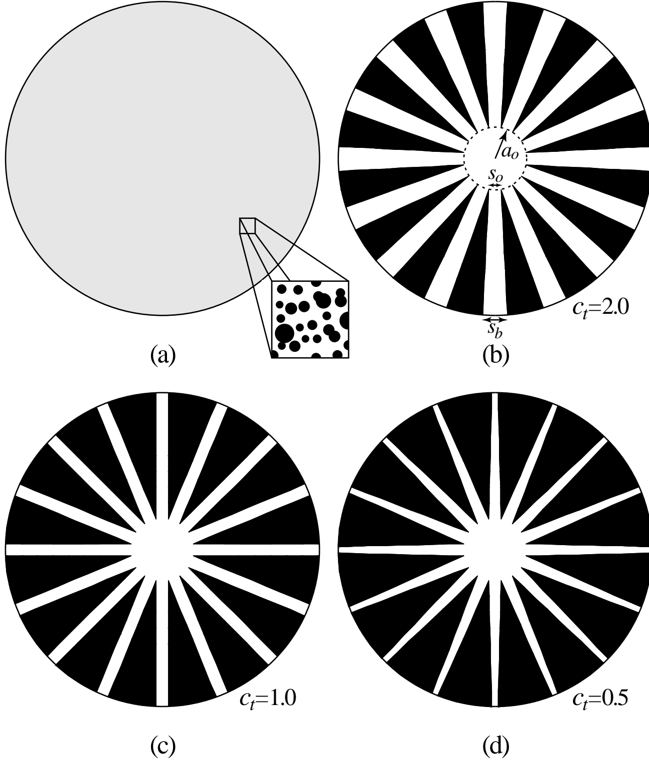

Fig. 4. Etch patterns examined in the current work. The black areas indicate etched (non-bonding) regions. (a) An array of small distributed holes resulting in uniform reduction in bonding area. (b) Spoke pattern showing the geometry definitions. The pattern is defined in terms of a_o and the taper ratio $c_t = s_b/s_o$. Taper ratio of $c_t = 2.0$ is shown. (c) Spoke pattern with $c_t = 1.0$. (d) Spoke pattern with $c_t = 0.5$.

The second type of pattern considered in the current work is designed to demonstrate how a pattern density that changes with radial position affects bonding. The basic geometry is shown in Fig. 4(b) and the pattern is defined in terms of the radius a_o, the outer radius b, and the taper ratio c_t. The taper ratio is given in terms of the arc length of bonding area at radius a_o, s_o, and the arc length of bonding area at b, s_b. The values of taper ratio, $c_t = s_b/s_o$, are limited to $0 \leq c_t \leq b/a_o$, where the case of $c_t = b/a_o$ corresponds to the case of an un-patterned wafer. Figures 4(b)-(d) show patterns with three different taper ratios. The bonding area as a function of bond front position can be written as

$$A = \begin{cases} \pi a^2 & a \leq a_o \\ \pi a_o \left[a_o + (a - a_o)\left(2 - (1 - c_t)\frac{a-a_o}{b-a_o}\right)\right] & a \geq a_o \end{cases} . \tag{23}$$

Evaluating the term da/dA for this case and using Eq. (12), the strain energy accumulation rate for the spoke pattern when $a \geq a_o$ is

$$\left(\frac{dU_E}{dA}\right)_{spoke} = \frac{(R/R_o)(1 - R_o)}{(1 - R) + c_t(R - R_o)} \left(\frac{dU_E}{dA}\right)_{blank}, \tag{24}$$

where $R_o = a_o/b$.

If the features are deep, not only is the bonding area reduced, but the stiffness is as well due to the large removal of material. The reduction in stiffness that is caused by cavities obviously depends on the exact pattern. However, to demonstrate the basic effect of deep etched features, a porous material model can be used to estimate the reduction in modulus with removal of material. Numerous models exist in the literature that predict the change in elastic properties with porosity. In the current work, a model, which assumes randomly distributed spherical voids is used. The effective elastic modulus, $\bar{E}$ and Poisson's ratio, $\bar{\nu}$ are given as

$$\bar{E} = E\left(\frac{p_v - p_o}{1 - p_o}\right)^m, \tag{25}$$

$$\bar{\nu} = \nu + \frac{1 - p_v}{1 - p_1}(\nu_1 - \nu), \tag{26}$$

where p_v is the volume fraction of solid material, and p_o, p_1, m, and ν_1 are constants that depend on the geometry [15]. For the case of randomly distributed spherical pores, $p_o = 0.182$, $p_1 = 0.160$, $m = 1.65$, and $\nu_1 = 0.221$, [15]. It should be noted that when the Poisson's ratio is near 0.2, which is common for many semiconductor materials, the effective Poisson's ratio does not change significantly with void fraction. Defining the etch volume fraction as $c_v = (1 - p_v)$ and noting that for well distributed holes $c_a = c_v$, the strain energy accumulation rate for deep etched wafers can be written as

$$\left(\frac{dU_E}{dA}\right)_{deep} = \frac{1}{p_v}\left(\frac{p_v - p_o}{1 - p_o}\right)^m \left(\frac{dU_E}{dA}\right)_{blank}. \tag{27}$$

This expression incorporates the reduction in stiffness and the reduction in bonding area due to the deep etches. However, it assumes the Poisson's ratio does not change as a result of the removal of material.

V. Experimental

To validate the model, experiments are being performed by bonding wafers with known bow to wafers with a specially designed etch pattern. Test wafers with various curvatures were fabricated by depositing a residually stressed (tensile) LPCVD silicon nitride film on the wafer and subsequently removing the film from the front surface. Wafers with varying film thicknesses, ranging from 0.18 to 0.57 μm, were fabricated, resulting in wafers with radius of curvatures from 14 to 50 m. The set of wafers that was bonded to the wafers with defined curvature were etched to define a test pattern. The etched wafers were fabricated by dry etching a shallow pattern on the bonding surface. The pattern chosen for the initial experiments was a spoke type pattern similar to those shown in Figs. 4(b)-(d). The actual pattern used has an initial radius, $a_o = 7$ mm, and a taper ratio, $c_t = 0.3$. All wafers that were used were 100 mm diameter n-type (100) silicon wafers with thicknesses ranging from 0.4 mm to 1.0 mm. Wafers were bonded at room temperature and bond front propagation was observed using a IR transmission setup.

VI. Results and Discussion

The primary quantity of interest from the analysis is the strain energy accumulation rate, dU_E/dA. If this quantity is less than the work of adhesion then bonding will occur, if it is not, then the bond front will not advance. The strain energy

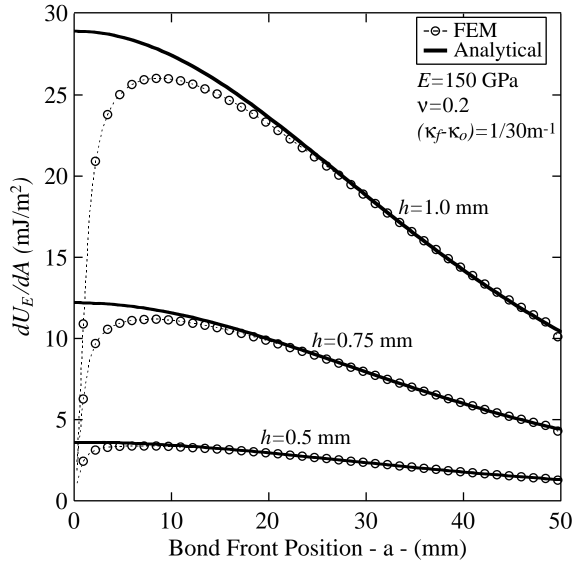

Fig. 5. Plot of strain energy accumulation rate, comparing analytical and finite element results for the specific case of 100 mm diameter wafers, where $E = 150$ GPa, $\nu = 0.2$, and $(\kappa_f - \kappa_o) = 1/30\ \text{m}^{-1}$.

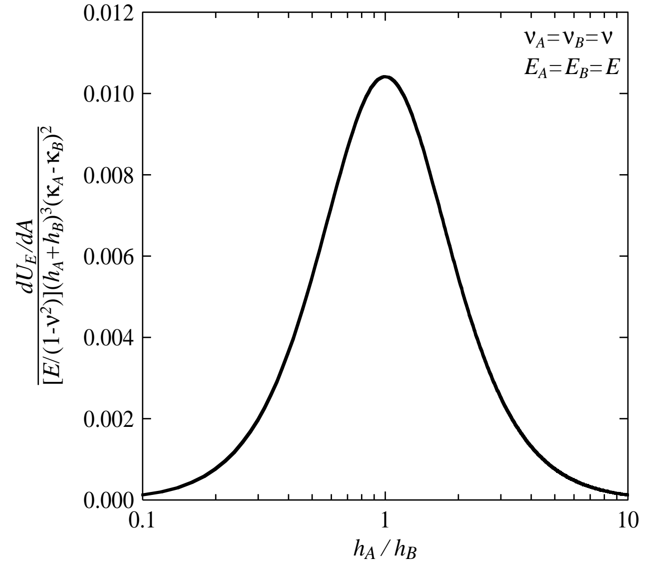

Fig. 6. Total strain energy accumulation rate (maximum accumulation rate, bond front at $R = 0$) for bonding two bowed wafers as a function of the thickness ratio of the wafers.

accumulation rate is plotted as a function of radial position on the wafer in Fig. 5 for a typical case of bonding a 100 mm diameter silicon wafer with a $\approx 40\ \mu$m bow to a rigid flat wafer (equivalent to a wafer mounted on a vacuum chuck). Analytical results were calculated using Eq. (15) and finite element results were obtained through the procedure outlined in section III-B. The finite element and analytical results match well when the bond front position is greater than 15 mm. The deviation between the two solutions at shorter bond front positions is a result of the fact that the plate theory used in the analytical solution does not accurately capture the stress state in the wafers when a is small. The finite element results show, as we may expect from similar problems in fracture mechanics, that the strain energy accumulation rate approaches goes to zero as a goes to zero. While the discrepancy means that the analytical mode over predicts the maximum strain energy accumulation rate by $\approx 10\%$, it still provides a closed form solution over the majority of the wafer that is useful in understanding the bonding process.

Figure 5 and Eq. (15) demonstrate some important characteristics of the bonding process. First, the strain energy accumulation rate decreases as the bond front advances further on the wafer. This suggests that it becomes easier to bond as the front advances, thus if the bond front advances more than $\approx$ 10 mm (the location of the peak strain energy accumulation rate) the wafer pair should bond completely. The other important point to note from Fig. 5 and Eq. (15) is the relative influence of the material properties and the geometry of the wafers. It is seen that the strain energy accumulation rate depends linearly on elastic modulus, the square of the curvature, and the cube of thickness. This strong dependence on thickness means that small increases in wafer thickness make it significantly more difficult to bond and that multi-wafer bonding is inherently more difficult. Furthermore, the dependence on modulus suggests that attempts to incorporate stiffer materials, such as SiC or Al_2O_3, will require tighter flatness control than is required when bonding silicon wafers. Finally, Eqs. (15) demonstrates that bonding difficulty is independent of wafer diameter. However, larger diameter wafers are in general thicker and hence may be more difficult to bond. It should be noted that the expression for strain energy accumulation rate is only independent of wafer diameter when written in terms of curvature (or radius of curvature) and that there is a dependence on wafer diameter when the shape is defined in terms of the bow, $\delta_i = \frac{1}{2}b^2\kappa_i$.

The scaling with thickness and modulus is also seen in the total strain energy accumulation rate for a pair of wafers given by Eq. (19). The normalized total strain energy accumulation rate for a pair is plotted in Fig. 6 as a function of thickness ratio. It has been normalized with respect to the total thickness, thus the plot demonstrates how the relative thickness of two wafers being bonded affects the strain energy accumulation rate for a stack of a given thickness. As is seen in Fig. 6, it is hardest to bond when the two wafers being bonded have equal thicknesses. This suggests that it is always desirable to have one wafer that is more compliant when bonding. This has important implications for attempting to use multiple wafer bonding steps to create MEMS structures. For instance, if a six wafer device is to be fabricated, as has been done, [16] it is preferable to add wafers to the stack individually rather than trying to make two three-wafer sub-stacks that then must be bonded.

While predicting whether or not bonding will occur is important, it is also critical that the geometry of the wafer after bonding be predictable. This is needed not only to calculate the strain energy accumulation rate for the wafers being bonded, but is also critical if subsequent bonding steps will be performed. Equation (18) gives the equilibrium curvature value as a function of the material properties and geometry of the wafers. The final curvature of a two wafer stack is plotted

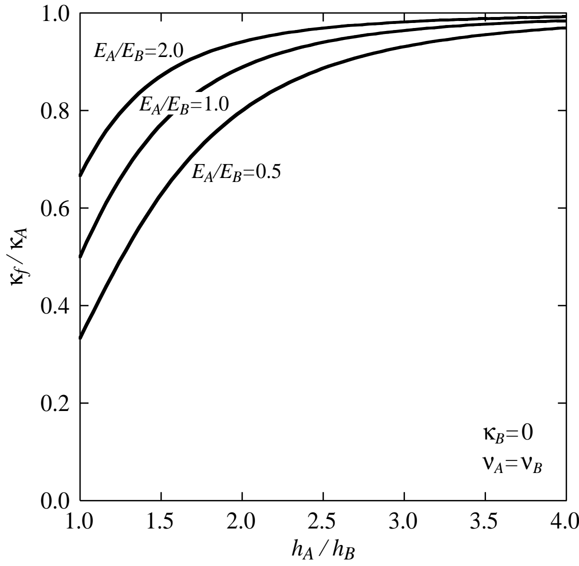

Fig. 7. The final curvature of a bonded stack given as a function of the thickness ratio and modulus ratio of the two wafers being bonded. One wafer is taken to be flat initially ($\kappa_B = 0$) and the wafers are assumed to have equal values of Poisson's ratio.

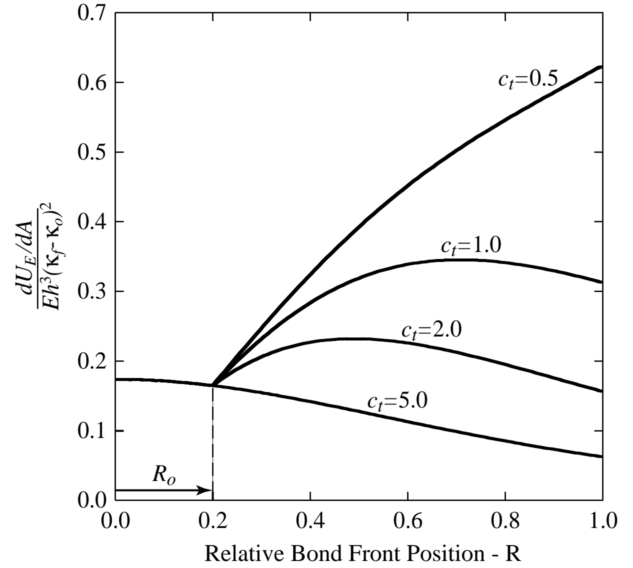

Fig. 8. Effect of spoke patterns with various taper ratios on strain energy accumulation rate. The case of $c_t = 5.0$ corresponds to the case of blank wafer for $R_o = 0.2$. A decreasing taper ratio increases the strain energy accumulation rate.

for various thickness and modulus ratios in Fig. 7. It is clear that the thicker wafer in the pair dominates the final curvature and the modulus ratio only plays an important role when the wafers have similar thicknesses. This result implies that it may be beneficial to measure wafer curvatures prior to bonding, and possibly match wafers to minimize the curvature of the stack. This is critical when a process flow involves multiple wafer bonding steps because maintaining flat stacks is essential in preventing bonding failure in the later steps.

Figures 8 and 9 demonstrate the profound effect that etch features can have on bonding. The strain energy accumulation rate for the spoke pattern, shown in Figs. 4(b)-(d), (assuming $R_o = 0.20$) for three different taper ratios, $c_t = 0.5$, $c_t = 1.0$, $c_t = 1.0$, was calculated as a function of bond front position using Eq.(24) and plotted in Fig. 8. From the plot, it is seen that these etch patterns can cause the strain energy accumulation rate to increase as the bond front approaches the wafer edge. This is important because it suggests that it becomes harder to bond as the front advances. Thus, blank wafers that can be bonded may only bond over a certain region once patterned. It should be noted that while these patterns were chosen due to their symmetry, a similar effect could be observed with a wafer where the feature density increases near the edges.

The results shown in Fig. 9 compare the effect of shallow features to deep features. The results were generated using Eqs. (22) and (27) and assume small, distributed etched features. It is evident from Fig. 9 that while shallow features make it more difficult to bond, wafers with deep features are easier to bond despite the reduction in bonding area. The reduction in stiffness caused by the material removal dominates over the reduction in bonding area.

The results shown in Figs. 8 and 9 have important design implications. These results suggest that the distribution of devices over a wafer can significantly effect the ability to

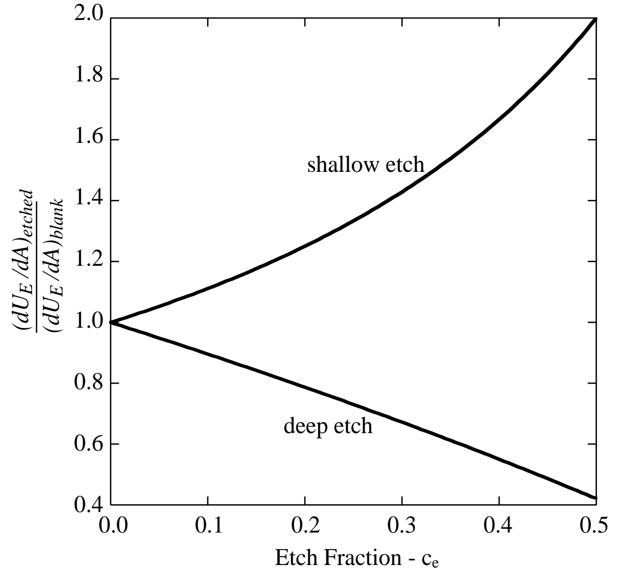

Fig. 9. The effect of distributed deep and shallow features on strain energy accumulation rate.

bond the wafers and as such pattern layout should be carefully considered. Furthermore, it may be possible to increase the ability to bond pairs of wafers by removing additional material between devices in order to increase the wafer compliance.

Experimental results at this point are preliminary, but encouraging. Figure 10 shows two different bonding pairs used in the experiments. The wafers in the two pairs have the same thickness, 525 μm, but have different curvatures. One wafer in each bonded pair is nominally flat and has the test pattern etched on it, while the other has a curvature that is a result of the tensile stressed film on the wafer back surface. In the pair pictured in Fig. 10(a), the bowed wafer has a radius of curvature of 14 m, while in Fig. 10(b), the bowed wafer has

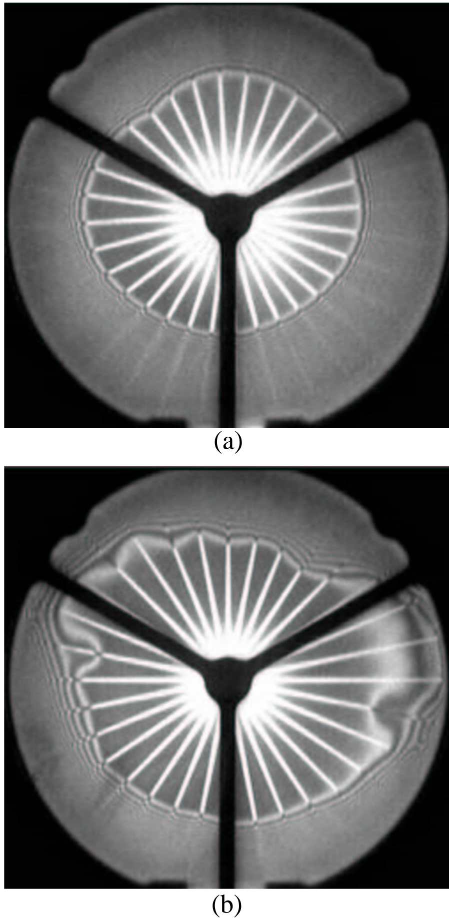

Fig. 10. IR images of two bonded wafer pairs. Both pairs are composed of a patterned wafer, which is nominally flat, bonded to a wafer with a defined bow. The bowed wafer in (a) has a radius of curvature of 14.2 m, while that in (b) has a radius of curvature of 23.3 m. As expected the bond front propagates further in (b) due to the decreased bow.

a radius of curvature of 23 m. It is clearly observed that the bond front propagates further when the radius of curvature is larger (the wafer is flatter). This is consistent with what is expected based on the modeling. In addition, pairs consisting of wafers with equal curvatures, but different thicknesses were bonded. The experimental results demonstrated that the bond front for the thinner wafer pair propagated further than that in the thicker wafer pair, as expected. While the trends are consistent with the model for both of these cases, the bond front propagation is not always axisymmetric, as seen in Fig. 10(b). Since the model was developed assuming axisymmetric propagation, quantitative agreement between the model and these experiments has not yet been achieved. Models that account for non-axisymmetric propagation are being developed and test wafers with improved geometry are being fabricated to try to achieve better quantitative agreement between the model and the experiments.

VII. Conclusion

A general bonding criterion based on the competition between the work of adhesion and the strain energy required to deform the wafers has been described. This criterion can be used to evaluate a range of flatness deviations and can account for the effect of etch patterns on bonding. The implementation of this bonding criterion has been demonstrated for the case of bonding bowed wafers. A closed form solution has been developed for the strain energy accumulation rate of bowed wafers and verified using finite element analysis. The results show that, when bonding un-patterned bowed wafers, if the bond front begins to advance it will propagate to the edge of the wafers. However, it was also demonstrated that etched features can alter this situation, and in some cases, it may become more difficult to bond as the bond front approaches the edge. In addition, the effect of deep etched features has been examined and it was demonstrated that their presence may facilitate bonding by lowering the strain energy accumulation rate. Finally, results from preliminary experiments are consistent with the model, however work is ongoing to achieve quantitative correlation.

References

[1] A. Mirza and A. Ayon, "Silicon wafer bonding: key to high-volume manufacturing," *Sensors*, December 1998.

[2] R. Khanna, August 2002, personal communication.

[3] N. Miki, August 2002, personal communication.

[4] J. Lasky, S. Stiffler, F. White, and J. Abernathy, "Silicon-on-insulator (SOI) by bonding and etch-back," in *International Electron Devices Meeting. Technical Digest*. IEEE, 1985, pp. 684–687.

[5] Q.-Y. Tong and U. Gosele, *Semiconductor wafer bonding : science and technology*. New York: Wiley, 1999.

[6] A. Plößl and G. Kräuter, "Wafer direct bonding: tailoring adhesion between brittle materials," *Materials Science and Engineering*, vol. R25, pp. 1–88, 1999.

[7] Q.-Y. Tong and U. Gösele, "Semiconductor wafer bonding: recent developments," *Materials Chemistry and Physics*, vol. 37, pp. 101–127, 1994.

[8] R. Stengl, K. Mitani, V. Lehmann, and U. Gosele, "Silicon wafer bonding: Chemistry, elasto-mechanics, and manufacturing," *Proceedings of the 1989 IEEE SOS/SOI Technology Conference*, pp. 123–24, 1989.

[9] Q.-Y. Tong and U. Gösele, "Thickness considerations in direct silicon wafer bonding," *J. Electrochem. Soc.*, vol. 142, pp. 3975–3979, 1995.

[10] H. Yu and Z. Suo, "A model of wafer bonding by elastic accomodation," *J. Mech. Phys. Solids*, vol. 46, pp. 829–844, 1998.

[11] C. Gui, M. Elwenspoek, N. Tas, and J. Gardeniers, "The effect of surface roughness on direct wafer bonding," *J. Appl. Phys.*, vol. 85, pp. 7448–7454, 1999.

[12] K. Turner and S. Spearing, "Modeling of direct wafer bonding: Effect of wafer bow and etch patterns," *J. Appl. Phys.*, vol. 92, no. 12, 2002, to be published, December.

[13] S. Timoshenko and S. Woinowsky-Krieger, *Theory of Plates and Shells*, 2nd ed. London: McGraw Hill, 1959.

[14] *ABAQUS Standard Users Manual*. Pawtucket, RI: Hibbitt, Karlsson, Sorensen, Inc., 2001.

[15] A. Roberts and E. Garboczi, "Computation of the linear elastic properties of random pourous materials with a wide variety of microstructure," *Proc. R. Soc. of London, Ser. A*, vol. 458, pp. 1033–1054, 2002.

[16] A. Mehra, A. Ayon, I. Waitz, and M. Schmidt, "Microfabrication of high-temperature silicon devices using wafer bonding and deep reactive ion etching," *Journal of Microelectromech. Syst.*, vol. 8, pp. 152–160, 1999.

Acknowledgment

All microfabrication and experiments were performed in the Microsystems Technology Laboratory at MIT, the help of the staff is greatly appreciated. The authors would also like to thank N. Miki and R. Khanna of the MIT microengine program for providing the pictures in Fig. 1.